Eur. Phys. J. B **12**, 479–491 (1999)

THE EUROPEAN PHYSICAL JOURNAL B

EDP Sciences

High temperature phase transitions in the crystal of p-trimethylammoniumbenzenesulfonate zwitterion

J. Even[1], M. Bertault[1,a], L. Toupet[1], A. Girard[1], and W.J. Kusto[2]

[1] Groupe Matière Condensée et Matériaux[b], Université de Rennes 1, Campus de Beaulieu, 35042 Rennes Cedex, France
[2] Institute of Physical and Theoretical Chemistry, Technical University of Wroclaw, 50-370 Wroclaw, Poland

Received 21 October 1998 and Received in final form 14 April 1999

Abstract. Crystals of *p*-trimethylammoniumbenzenesulfonate (ZWT) have been obtained from the thermally induced solid−state reaction of methyl *p*-dimethylaminobenzenesulfonate (MSE) or by recrystallization in aqueous solution. The characterization of four crystalline phases has been performed by calorimetric, birefringence, X-ray and Raman scattering studies. An unknown phase transition at room temperature yielding a new crystallographic phase has been found by calorimetric measurements. ZWT crystalline samples obtained from the MSE → ZWT solid state reaction are disordered as compared to ZWT single crystals obtained by growing from aqueous solution. This disorder is related to different arrangements of the phenyl ring orientations.

PACS. 61.50.Ks Crystallographic aspects of phase transformations; pressure effects – 61.66.Hq Organic compounds – 65.40.+g Heat capacities of solids

1 Introduction

A single crystal or a polycrystalline powder of methyl *p*-dimethylaminobenzenesulfonate (MSE) is converted to the zwitterionic product *p*-trimethylammoniumbenzenesulfonate (ZWT) by a thermally induced solid−state methyl-transfer reaction [1]. The chemical equation of the reaction process is shown in Figure 1. Recent papers [2–9] have shown the influence of the crystal field on a topochemical reaction. The reaction MSE → ZWT is associated to a first order ferroelastic phase transition [5] which takes place in partially reacted MSE crystal when going from the monoclinic structure of pure MSE [1,2] to the orthorhombic structure of pure ZWT [1,3]. The differences between the crystalline structures of pure MSE and pure ZWT are due to the large electric dipolar interactions between the ZWT molecules [2,3]. It has been recently shown by theoretical calculations [8] that these interactions are also the driving force for the chemical reaction itself: the MSE molecule is energetically more stable than the ZWT molecule but the ZWT crystal is energetically more stable than the MSE crystal.

Then a better knowledge of the crystalline structures of both pure MSE and pure ZWT crystals will enable a detailed analysis of the reaction. From one of our previous studies [4], we know that phase transitions are observed only at low temperatures in pure MSE crystals. In pure ZWT crystals, the experimental situation is more tricky to describe. Indeed, pure ZWT crystals obtained directly from the MSE → ZWT reaction are always disordered by large plastic deformations: they occur when the mixed MSE → ZWT crystal undergoes the structural instability which takes place during the thermal transformation [5]. Fortunately, Sukenik *et al.* [1] obtained crystals of pure ZWT by recrystallization from aqueous solution. By studying oscillation and Weissenberg X-ray photographs, these authors found that the crystals had an orthorhombic structure with $a = 10.15$ Å, $b = 20.55$ Å and $c = 9.69$ Å at room temperature. The space group was either Pbam or Pba2. Good compatibility was found between the powder diffraction patterns of these ZWT crystals and the ones of the ZWT polycrystalline powders obtained by complete reaction of MSE polycrystalline powder. Sarma *et al.* [3] showed that three crystalline phases could be identified. They used crystals grown by slow evaporation of water-methanol solutions; these crystals were mostly twinned. A low-temperature α-phase of orthorhombic Pnc2 symmetry (8 molecules in the unit cell) was accurately determined at $T = 193$ K. For the intermediate β-phase, a formal space group Pbma (4 molecules in the unit cell) was proposed by neglecting some reflections or satellites (in particular along the c^* axis). At room temperature, a coexistence of α-phase and β-phase was observed. Finally, at 385 K, a tetragonal structure (γ-phase) was found from precession X-ray photographs. The authors have proposed the space group P4/nmm (2 molecules in the unit cell) again by neglecting streaks with half-integer l in the c^* direction.

[a] e-mail: marcel.bertault@univ-rennes1.fr
[b] UMR CNRS 6626

Experimentally, the thermally activated MSE → ZWT reaction is studied above room temperature, usually around $T = 330$ K in the [310 K–350 K] temperature interval. In this temperature range the crystalline structure of pure ZWT is only roughly known from previous studies [1,3]. The aim of this paper is then to present new results obtained from careful examination of the high temperature phase transitions in pure good quality ZWT crystals (obtained from aqueous solution) by experimental methods described in Section 2. These results have been obtained by calorimetry (Sect. 3), X-ray diffraction using both the precession method (Sect. 4) and diffractometry for structure determination (Sect. 5), Raman scattering (Sect. 6) and optical birefringence (Sect. 7). Comparisons are made with ZWT crystals obtained directly from the MSE → ZWT solid-state reaction. Section 8 is a discussion and a conclusion.

2 Experimental methods

2.1 Crystal growth

With the aim to prepare zwitterion, MSE crystals have been grown from acetone solutions and then have been thermally converted in ZWT as described by Sukenik *et al.* [1]. In our case, MSE crystals were thermally reacted in several DSC experiments to complete transformation in ZWT and then dissolved in pure water; after filtration the ZWT crystals have been grown by very slow evaporation of the aqueous solution (ten days) at room temperature.

The ZWT crystals obtained were colourless (001) plates (as verified by conoscopic polarized light observations [5]) of maximum thickness approximately equal to 0.5 mm. Sarma and Dunitz [3] obtained, from water-methanol solution, cube-like crystals twinned across the (110) face or untwinned plate-like crystals. On the other hand, Sukenik *et al.* [1] did not give any description of their ZWT crystals (probably very small) grown from aqueous solution. The mass of the largest monocrystal which we obtained was of the order of 6 mg.

2.2 Calorimetric measurements

Calorimetric experiments were performed on a Perkin Elmer DSC7 differential scanning calorimeter connected to a DEC 425 calculator. Temperatures were calibrated using (as the case may be) cyclohexane (transitions at $T = 186.1$ K and $T = 279.7$ K), *p*-nitrotoluene (melting point at $T = 324.7$ K) or indium (melting point at $T = 429.8$ K) as standards. Energy was calibrated using the enthalpy of melting of indium ($\Delta H = 28.45$ kJ/mole). Samples were carefully encapsulated in aluminium capsules for Cp measurements at a heating rate of 10 K/min. For the first order phase transitions, the transition temperature was calculated from the intersection of the peak onset and of the baseline. Several samples were used: some of them were made either with polycrystalline powder of ZWT obtained after complete thermal transformation of the starting MSE powder, or with ZWT samples including crystalline areas as obtained in several cases after thermal reaction of MSE monocrystals and as verified under the polarization microscope (see Sect. 3). The other samples used in this study were obtained as described in the previous Section 2.1: polycrystalline powder or plate-like monocrystals of ZWT were grown directly from a water solution of ZWT; in the DSC experiments, ZWT powder or several monocrystals (three or four with the aim of obtaining a mass in the order of ten milligrams) or only one monocrystal (of about 6 mg) were carefully encapsulated in aluminium capsules.

2.3 X-ray diffraction

The X-ray diffraction photographs were obtained with a precession apparatus using the Cu-K_α line ($\lambda = 1.542$ Å) after filtering through a graphite monochromator (precession angle $\mu = 30$ degrees) at four temperatures: $T = 253$ K, 295 K, 323 K and 400 K. Structural data collection was performed with an Enraf-Nonius CAD-4 diffractometer. Structures were refined with the SHELXL93 program [10,11]. Complete structure determination was performed at five temperatures on a ZWT single crystal grown from aqueous solution (size $0.4 \times 0.33 : 0.16$ mm): $T = 100$ K, $T = 255$ K, $T = 333$ K, $T = 375$ K and $T = 400$ K. For recording the low-temperature structures and precession photographs the sample is kept cool by an Oxford Cryostream system using a nitrogen flow with temperature controlled to within 0.1 K. The high temperature structures and precession photographs were obtained by setting the crystal in a dry air flow controlled by a thermal resistance to within 0.5 K.

Lists of atomic positional and displacement parameters, torsion angles and structure factors for low and high temperature structures of the α, β and γ phases of monocrystalline zwitterion have been deposited at the Cambridge Crystallographic Data Centre (CCDC), 12, Union Road, Cambridge CB2 1EZ, UK.

2.4 Raman scattering experiment

The Raman spectra were recorded with a Dilor XY micro-Raman spectrometer using a Ti-Sa laser at $\lambda = 7\,185$ Å with an incident light power equal to about 25 mW. The Raman spectra were recorded using a multichannel CCD detector cooled to 77 K. It was equipped with a Linkam TMS90 heating/freezing system used for *in situ* study of ZWT crystals either for isothermal experiments, or for scanning temperature experiments (scanning rate from 0.1 °C/min to 20 °C/min). The spectra were recorded in a backscattering geometry. It was not possible to obtain polarized spectra with this experimental setting (when using the micro-Raman spectrometer with convergent polarized beam through very small ZWT samples the experimental tests were not conclusive).

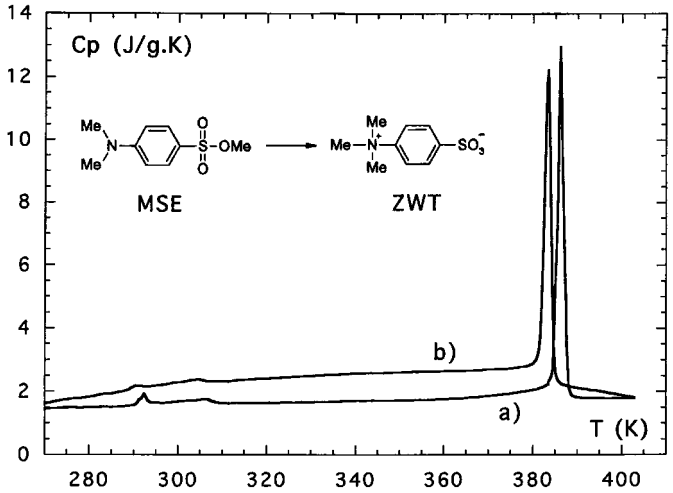

Fig. 1. Evolution of the specific heat of a ZWT single crystal (a) and of ZWT powder (b) as a function of temperature in the [270–410 K] temperature range. Three endotherms are observed both in (a) and (b). Chemical equation of the reaction is drawn on the figure.

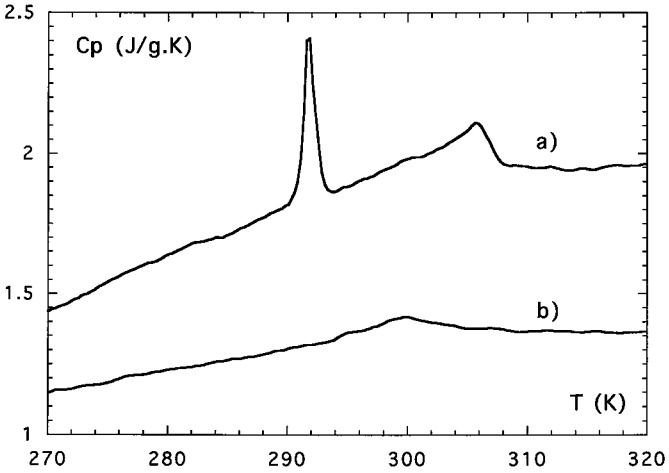

Fig. 2. (a) Enlarged view (in the [270–320 K] temperature range) of the first two endotherms (Fig. 1a) observed in the ZWT single crystal. (b) Enlarged view (in the [270–320 K] temperature range) of the only one corresponding endotherm observed in the ZWT sample obtained by thermal transformation of a MSE single crystal and shown in Figure 3.

2.5 Optical birefringence

Optical properties of ZWT single crystals reported here were studied using polarizing research microscopes equipped with numerous supporting optical accessories (like an universal stage, tilting compensators and many others) [12] and a Linkam THM600 heating/cooling stage (temperature stability of approximately 0.1 °C).

3 Calorimetric results

3.1 ZWT crystals grown from aqueous solution

Figure 1 shows the variation of the specific heat of a ZWT single crystal ($m = 5.71$ mg, Fig. 1a) and of ZWT powder ($m = 9.26$ mg, Fig. 1b) as a function of temperature in the [270 K–410 K] temperature range. The common feature is that three endotherms are observed. Figure 2a shows an enlarged view of the first two endotherms for the ZWT single crystal (studied in Fig. 1a) in the [270 K–320 K] temperature interval. At $T_1 = 291$ K, a first-order like transition is observed. The enthalpy associated to this endotherm is equal to 0.73 J/g. At $T_2 = 307$ K a second-order like phase transition is observed. The specific heat jump at T_2 is equal to 0.16 J/g K. These new experimental results indicate clearly that an unknown crystallographic phase exists between the α-phase ($T < T_1 = 291$ K) and the β-phase ($T > T_2 = 307$ K); this intermediate phase will be named hereafter the I-phase. From Figure 1b, we can see that the first order transition is rounded and smoother in ZWT powder as compared to the one in a ZWT single crystal (Fig. 1a).

A third very sharp endotherm is observed at $T_3 = 386$ K (Fig. 1a): it corresponds to the first order phase transition between the β-phase and the γ-phase [3]. The enthalpy associated with this transition is equal to $\Delta H = 19.2$ J/g, to be compared to the value of 10.2 J/g found by Sarma *et al.* [3]. In ZWT powder (Fig. 1b), this endotherm is somewhat less sharp and also shifted to a slightly lower temperature.

We should emphasize here that before performing experimental studies on ZWT samples grown from aqueous solution, we have carefully checked that no water is included in the matrix. This is easy to verify by DSC (Fig. 1) on the endotherms at 273 K and 373 K where there is no indication of the melting and boiling points of water. Residual water can be removed either for the most part by keeping the samples at room temperature during several weeks or totally by heating above 373 K.

3.2 ZWT crystals obtained from the thermally reacted MSE monocrystals

From one of our previous experimental studies [5], we know that the large plastic deformations induced by the structural instability which takes place at intermediate MSE → ZWT crystal conversion may lead either to breaking the crystal into pieces (ZWT crystalline powder is obtained) or to ZWT crystals retaining good crystallinity. All the intermediate cases between these two extremes can be observed. Figure 3 shows the variation of the heat capacity of a ZWT crystal retaining good crystallinity ($m = 9.71$ mg) as a function of temperature in the [270 K–410 K] temperature range. This sample has been obtained by thermal transformation of a MSE single crystal after heating from 303 K to 423 K at 0.1 K mm^{-1}. In the [270 K–320 K] temperature interval (Fig. 2b) only one broad endotherm at about 298 K is observed in this case, instead of two endotherms at $T_1 = 291$ K and $T_2 = 307$ K in ZWT single crystals grown from aqueous

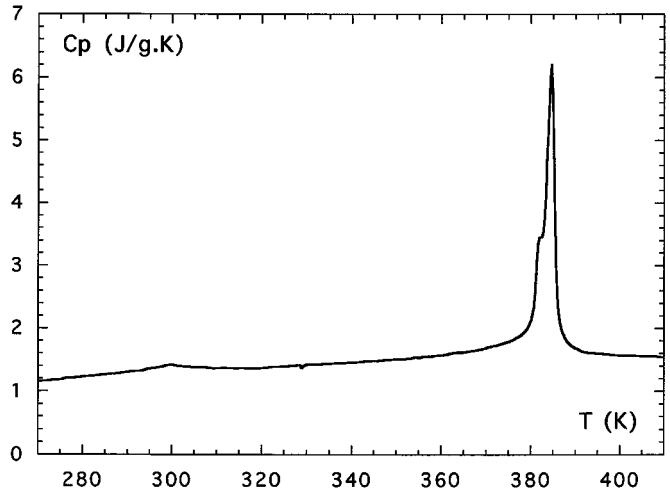

Fig. 3. Evolution, as a function of temperature in the [270–410 K] temperature range, of the specific heat of a ZWT sample obtained by thermal transformation of a MSE single crystal. Two endotherms are observed at about 300 and 390 K.

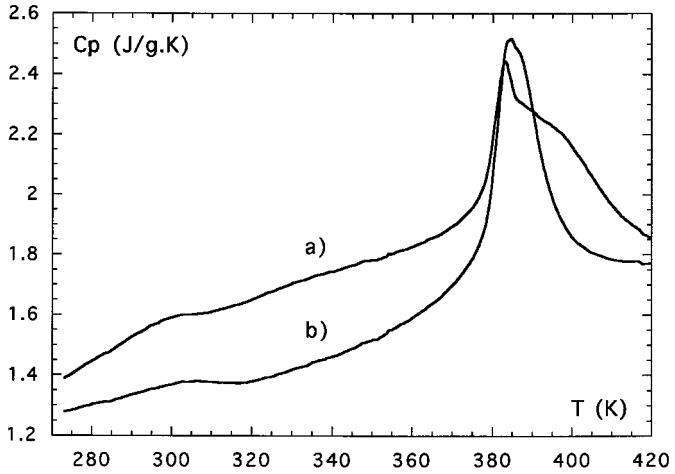

Fig. 4. Evolution, as a function of temperature in the [270–420 K] temperature range, of the specific heat of a ZWT powder obtained by thermal transformation of a MSE single crystal. In the first DSC scan (a) a broad endotherm is observed around $T_3 = 383$ K; in the second scan (b) above, a sharper endotherm at T_3 appears.

solution (Sect. 3.1, Fig. 2a). The experimental signature of the first order phase transition between the β-phase and the γ-phase (Sect. 3.1) is a sharp endotherm at about $T_3 \approx 383$ K. This endotherm is however less sharp than in water-grown ZWT single crystals (Fig. 1a): the maximum of Cp is about twice as smaller. The enthalpy associated to this endotherm $\Delta H = 13.1$ J/g is in good agreement with those of Section 3.1, $\Delta H = 19.2$ J/g.

Our calorimetric study of ZWT powders obtained from the MSE → ZWT solid state isothermal reaction at about 340 K proves that thermal history is a key factor in these samples. Figure 4 illustrates the first kind of phenomenon which is often observed. In the first DSC scan (Fig. 4a), a very broad endotherm is observed around 298 K but also around $T_3 \cong 383$ K and above. In the second scan (Fig. 4b), a sharper endotherm at T_3 appears. For all the following scans, the situation remains unchanged (Fig. 4b). The enthalpy of the endotherm at T_3 is equal to $\Delta H = 10.0$ J/g (Fig. 4b). The maximum of Cp is much smaller than those obtained in the Figures 1 and 3. We point out that it is necessary to heat the ZWT powder up to 423 K to observe this phenomenon; if the sample is heated only to 403 K, DSC scans retained the first shape (Fig. 4a).

A second kind of phenomenon is sometimes observed in ZWT powders obtained by isothermal reaction in the [220 K–340 K] temperature range. On a first DSC scan recorded from 203 K to 393 K at 10 $\mathrm{K\,mm^{-1}}$, a very broad endotherm extending from about 250 K to 350 K is present. The usual situation is observed again on the following DSC scans: the first endotherm is now located around 298 K.

4 X-ray diffraction: precession methods

4.1 Introduction

In order to establish a better comparison between the crystallographic structures of the four phases of the ZWT crystal (α-phase, I-phase, β-phase and γ-phase), we decided to choose the orientation of the α-phase axes as the orientation of the crystallographic axes for all the four phases. Then we shall use h', k', l' letters for the reflection conditions corresponding to these common axes (named a', b', c'); h, k, l and a, b, c letters will be used for the "conventional" space groups used in Section 5 for the high temperature phases (I, β, γ) and for which the orientation of the crystallographic axes is different from that of the α-phase space group.

Then the reflection conditions of the Pnc2 space group of the α-phase are $h0l$ with $l = 2n$ and $0kl$ with $k + l = 2n$ ($a' = a$, $b' = b$, $c' = c$; $h' = h$, $k' = k$, $l' = l$). The reflection conditions of the $Pca2_1$ conventional space group of the β-phase are $h0l$ with $h = 2n$ and $0kl$ with $l = 2n$; when using axes $a' = a$, $b' = c$, $c' = b$ with $k' = l$, $l' = k$, the reflection conditions become $0k'l'$ with $k' = 2n$ and $h'k'0$ with $h' = 2n$. The reflection conditions of the $P4_2/ncm$ conventional space group of the γ-phase are $hk0$ with $h + k = 2n$ and $0kl$ with $l = 2n$; when using $a' = a - b$, $b' = a + b$ with $h' = h - k$, $k' = h + k$, the reflection conditions became $h'k'0$ with $h' = 2n$ and $k' = 2n$.

Sections 4.2, 4.3 and 4.4 show that the reflection conditions of the intermediate I-phase are $h'00$ with $h' = 2n$, $0k'0$ with $k' = 2n$ and $00l'$ with $l' = 2n$.

4.2 (a′, b′) plane

Figure 5 shows precession photographs obtained at respectively $T = 273$ K (α-phase), $T = 295$ K (I-phase), $T = 323$ K (β-phase) and $T = 400$ K (γ-phase). These photographs indicate that the four phases have different

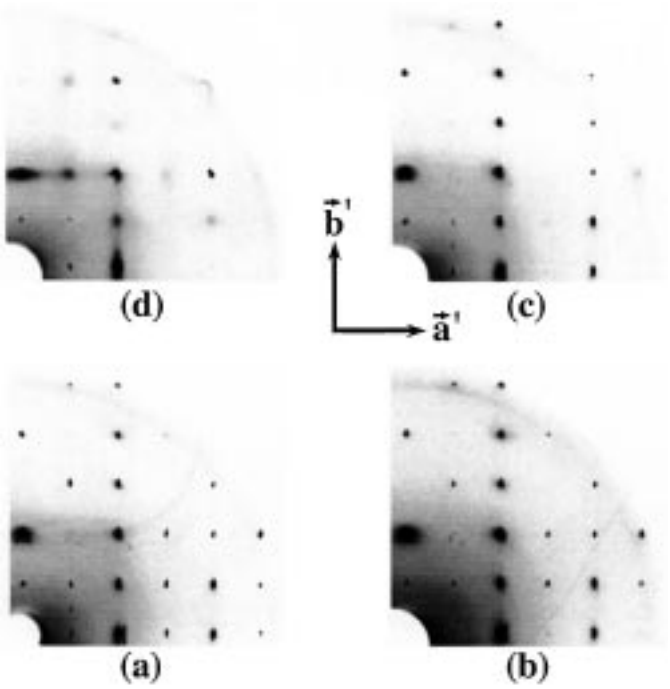

Fig. 5. Precession photographs obtained at (a) $T = 273$ K (α-phase); (b) $T = 295$ K (I-phase); (c) $T = 323$ K (β-phase); (d) $T = 400$ K (γ-phase) in the (a', b') plane. The four crystallographic phases have different X-ray scattering patterns in the (a', b') plane.

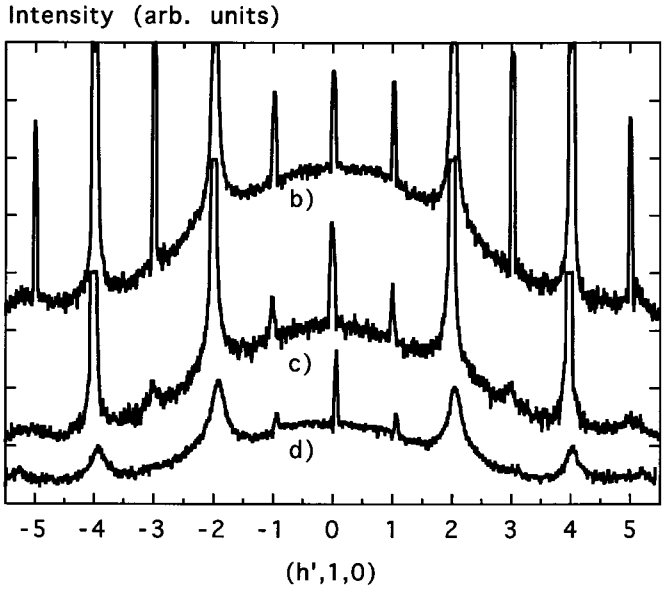

Fig. 6. Intensity profiles obtained along the $(h', 1, 0)$ direction and corresponding to the photographs of Figure 5: at (b) $T = 295$ K; (c) $T = 323$ K and (d) $T = 400$ K. The three central peaks $(0, 1, 0)$ and $(\pm 1, 1, 0)$ are associated to $\lambda/2$ scattering related to the strong Bragg peaks at $(0, 2, 0)$ and $(\pm 2, 2, 0)$ (Fig. 5).

X-ray scattering patterns in the (a', b') plane. Figure 6 shows intensity profiles along the $(h', 1, 0)$ direction corresponding to the photographs of Figure 5: for respectively $T = 295$ K, $T = 323$ K and $T = 400$ K. The profile corresponding to the α-phase is the same as that of the I-phase and it is not shown. The three central peaks $(0, 1, 0)$ and $(\pm 1, 1, 0)$ are associated to $\lambda/2$ scattering related to the strong Bragg peaks at $(0, 2, 0)$ and $(\pm 2, 2, 0)$ in Figure 5. Diffuse scattering is observed on profile (d) ($T = 400$ K) at $(\pm 2, 1, 0)$ and $(\pm 4, 1, 0)$ positions. This diffuse scattering transforms into Bragg peaks in profile (c). The difference between profiles (c) ($T = 323$ K, β-phase) and (b) ($T = 295$ K, I-phase) appears when considering the $(\pm 3, 1, 0)$ and $(\pm 5, 1, 0)$ positions: weak diffuse scattering is observed at $T = 323$ K whereas weak Bragg peaks are observed at $T = 295$ K. The difference between the α-phase ($T = 273$ K) and the intermediate I-phase ($T = 295$ K) appears along the $(h', 0, 0)$ direction in the photographs (a) and (b) of Figure 5. The $(1, 0, 0)$ spot is associated in both photographs to $\lambda/2$ scattering but Bragg peaks are located at $(3, 0, 0)$ and $(5, 0, 0)$ positions in photograph (a) whereas only small diffuse scattering is observed at the $(3, 0, 0)$ position in photograph (b). For giving a summary, we can write the reflection conditions in the (a', b') plane for $(h', k', 0)$ as follows: α-phase: $h' = 0$ with $k' = 2n$; I-phase: $h' = 0$ with $k' = 2n$ and $k' = 0$ with $h' = 2n$; β-phase: $h' = 2n$ and $h' = 0$ with $k' = 2n$; γ-phase: $h' = 2n$ and $k' = 2n$.

4.3 (b', c') plane

Figure 7 shows photographs obtained respectively at $T = 323$ K (β-phase) and at $T = 295$ K (I-phase). For the β-phase, in the (b', c') plane, the reflection conditions are $(0, k', l')$ with $k' = 2n$. For the I-phase, the reflection conditions are only $k' = 0$ with $l' = 2n$ and $l' = 0$ with $k' = 2n$. One may first notice that, in both phases, the c parameter is equal to about 20 Å (more precise determinations are given in Sect. 5) and is not reduced to about 10 Å as claimed by the authors of references [1,3]. Anyway, diffuse streaks along c^* are observed at room temperature by these authors (Ref. [3]): reflections with l odd increased in intensity when cooling from room temperature. In our work, Bragg reflections with l odd are observed in the four phases. Some diffuse scattering appears in the photographs at $T = 295$ K and $T = 323$ K (Fig. 7) mainly around the $(0, \pm 1, \pm 6)$ and $(0, \pm 1, \pm 10)$ positions. This diffuse scattering is distributed along the b' axis and is not related to the phase transition between the intermediate phase (Fig. 7b) and the β-phase (Fig. 7a). We did not make the photograph in the (b', c') plane for the α-phase to check whether this diffuse scattering is associated to the phase transition between the α-phase and the I-phase. However we know from previous crystallographic results [3] and the results given in Section 5.1 that reflection conditions for the α-phase are $(0, k', l')$ with $k' + l' = 2n$ and $k' = 0$ with $l' = 2n$. So, the $(0, \pm 1, \pm 6)$ and $(0, \pm 1, \pm 10)$ positions do not correspond to Bragg peaks in the α-phase. This diffuse scattering is probably due to defects in the lattice.

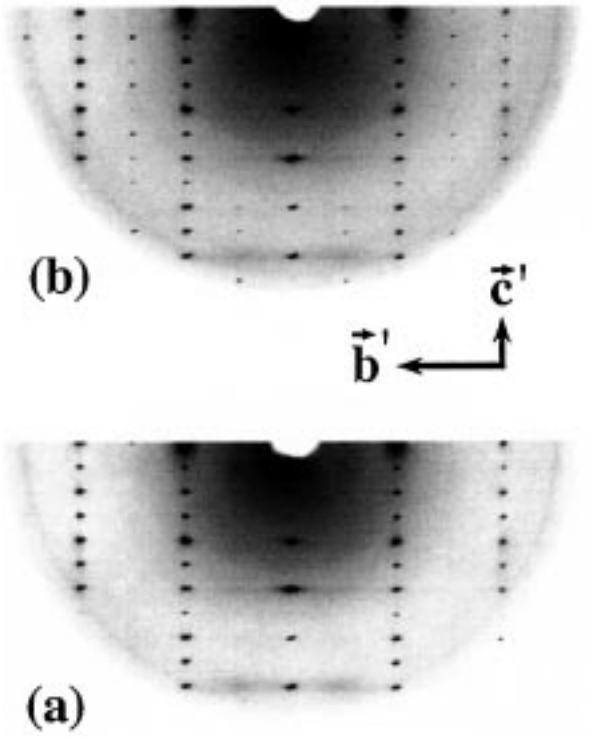

Fig. 7. Precession photographs at (a) $T = 323$ K (β-phase) and (b) $T = 295$ K (I-phase) in the (b', c') plane. For the β-phase the reflection conditions are $k' = 2n$. The c parameter is equal to about 20 Å in the four phases.

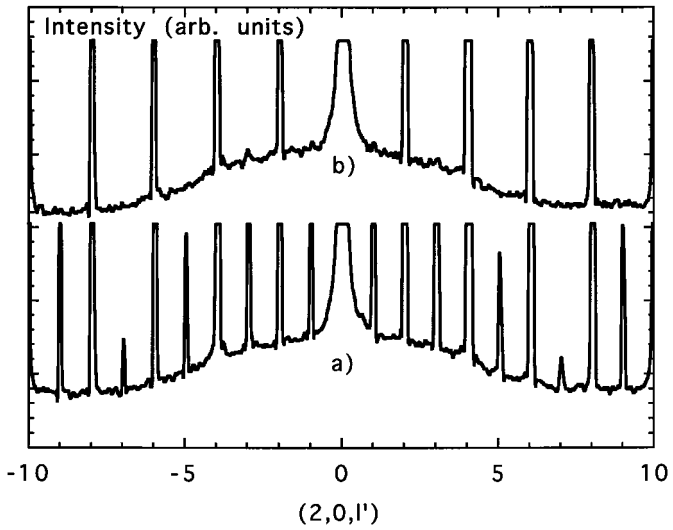

Fig. 8. Intensity profiles along the $(2, 0, l')$ direction at (a) $T =$ 295 K (I-phase) and (b) $T = 253$ K (α-phase). Bragg peaks with l' odd are not observed in the α-phase.

4.4 (a', c') plane

Figure 8 represents respectively intensity profiles along the $(2, 0, l')$ direction at $T = 295$ K (I-phase) and $T =$ 253 K (α-phase). It confirms that the reflection condition for the α-phase in the (a', c') plane is $(h', 0, l')$ with $l' = 2n$. On the contrary, Figure 8 shows that this reflection condition is not valid in the intermediate phase for which the reflection condition in this plane is $(0, 0, l')$ with $l' = 2n$.

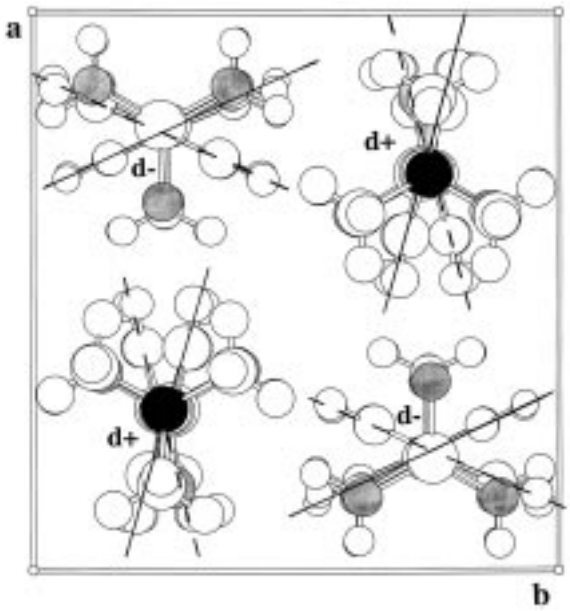

Fig. 9. Projection of two adjacent layers of molecules (contained in the same orthorhombic cell) along the c direction in the α-phase of a ZWT single crystal. The molecules are called d+ (electric dipole up) and d− (electric dipole down). The lines represent the orientations of the phenyl rings perpendicular to the (ab) plane; the dashed lines give the orientations in the lower layer, the full lines in the upper layer.

5 X-ray diffraction: crystallographic structures

5.1 α-phase

Complete structure determination of a ZWT monocrystal (see Sect. 2.3) was performed at two temperatures $T = 100$ K and $T = 255$ K (see Tab. 1). They correspond to the orthorhombic α-phase with the Pnc2 space group, 8 molecules in the unit cell ($Z = 8$) and 2 molecules in the asymmetric units. These results essentially confirm the ones obtained by Sarma *et al.* at $T = 193$ K [3]. Figure 9 shows the projection of two consecutive layers of molecules (parallel to the (a, b) plane) down the c axis in the same unit cell. In each stack along the c direction, all the zwitterions have the same orientation: the electric dipole is pointing up for the molecules having the nitrogen atom appearing in Figure 9 and the electric dipole is pointing down for the molecules having the sulfur atom appearing in Figure 9. The molecules can be called d+ (dipole up) and d− (dipole down) respectively. The most striking feature is that there is only one phenyl ring orientation for the d+ molecules and one phenyl orientation for the d− molecules in the same layer. For example, at $T = 100$ K, the angle between the phenyl ring orientations of the d+ and d− molecules in the lower layer (broken lines) is equal to about 50°. At $T = 255$ K, this angle is equal to 52°. The orientations of the phenyl rings of each kind of dipole

Table 1. Crystal data and summary of refined parameters for ZWT single crystal at $T = 100$ K and $T = 255$ K in the α-phase, at $T = 295$ K in the intermediate I-phase, at $T = 333$ K and $T = 375$ K in the β-phase and at $T = 400$ K in the γ-phase.

Temperature	100.0(2) K	255.0(2) K	295.0(2) K
Crystal system, space group	Orthorhombic, Pnc2	Orthorhombic, Pnc2	Orthorhombic
Unit cell dimensions	a = 10.078(8) Å	a = 10.138(8) Å	a = 9.535(10) Å
	b = 9.362(2) Å	b = 9.514(2) Å	b = 10.212(2) Å
	c = 20.847(3) Å	c = 20.872(3) Å	c = 20.832(5) Å
Volume	1967.1(16) $Å^3$	2013.1(17) $Å^3$	2028(2) $Å^3$
Z, Calculated density	8, 1.454 Mg/m^3	8, 1.421 Mg/m^3	8, 1.410 Mg/m^3
Absorption coefficient	0.309 mm^{-1}	0.302 mm^{-1}	0.300 mm^{-1}
F(000)	912	912	912
Limiting indices	0< h< 11,0< k< 11,0< l< 26	0< h< 8,0< k< 12,0< l< 26	0< h< 12,0< k< 13,0< l< 26
Reflections collected / unique	1985 / 1985	1769 / 1769	2508 / 2508
Data / restraints / parameters	1985 / 1 / 332	1769 / 1 / 332	2508 / 1 / 66
Goodness-of-fit on F^2	1.100	1.022	3.156
Final R indices [I>2sigma(I)]	R1 = 0.0323, wR2 = 0.0919	R1 = 0.0338, wR2 = 0.0948	R1 = 0.27
R indices (all data)	R1 = 0.0398, wR2 = 0.0963	R1 = 0.0503, wR2 = 0.1036	R1 = 0.34
Extinction coefficient	0.0015(4)	0.0010(4)	
Largest diff. peak and hole	0.601 and -0.420 e.$Å^{-3}$	0.425 and -0.258 e.$Å^{-3}$	

Temperature	333.0(2) K	375.0(2) K	400(2) K
Crystal system, space group	Orthorhombic, $Pca2_1$	Orthorhombic, $Pca2_1$	Tetragonal, $P4_2/ncm$
Unit cell dimensions	a = 10.198(3) Å	a = 10.224(3) Å	a = 7.195(4) Å
	b = 20.876(20) Å	b = 20.896(9) Å	
	c = 9.648(8) Å	c = 9.801(9) Å	c = 20.880(8) Å
Volume	2054(4) $Å^3$	2094.0(18) $Å^3$	1080.9(30) $Å^3$
Z, Calculated density	8, 1.392 Mg/m^3	8, 1.366 Mg/m^3	4, 1.323 Mg/m^3
Absorption coefficient	0.296 mm^{-1}	0.291 mm^{-1}	0.282 mm^{-1}
F(000)	912	912	456
Limiting indices	0< h< 13,0< k< 26,0< l< 12	0< h< 12,0< k< 26,0< l< 12	0< h< 9,0< k< 9,0< l< 26
Reflections collected / unique	2378 / 2378	2420 / 2420	1173/656 [R(int)=0.0342]
Data / restraints / parameters	2378 / 1 / 320	2420 / 1 / 320	656 / 0 / 54
Goodness-of-fit on F^2	1.028	1.037	1.523
Final R indices [I>2sigma(I)]	R1 = 0.0510, wR2 = 0.1415	R1 = 0.0533, wR2 = 0.1556	R1 = 0.1147, wR2 = 0.3927
R indices (all data)	R1 = 0.1061, wR2 = 0.1718	R1 = 0.1224, wR2 = 0.1909	R1 = 0.1749, wR2 = 0.4394
Extinction coefficient	0.0006(4)	0.0002(4)	0.000(6)
Largest diff. peak and hole	0.529 and -0.419 e.$Å^{-3}$	0.403 and -0.305 e.$Å^{-3}$	0.647 and -0.343 e.$Å^{-3}$

in a stack are different when considered in two consecutive layers (in fact they are symmetrical about b axis). So the angle between the phenyl rings of the d+ molecule in the lower layer and the d− molecule in the upper layer (or inversely between ring orientations of the d− molecule in the lower layer and the d+ molecule in the upper layer)

is equal to about 82°. These angles (82° and 50°) are respectively determined in Figure 9 by lines representing the mean projections of the phenyl rings of the d+ and d− molecules on the (a, b) plane.

5.2 Intermediate I-phase

Data acquisition was performed at room temperature (T = 295 K) with three different ZWT single crystals. We checked by differential scanning calorimetry that each of these single crystals undergo the two structural first order and second order phase transitions which mark the bounds of the intermediate I-phase at T_1 = 291 K and T_2 = 307 K (Fig. 2a). 2 508 reflections were observed with $I \geq 2\sigma(I)$ but it was not possible to obtain an acceptable refinement of the crystallographic structure (see Tab. 1). That is why we must consider several assumptions.

First, we assumed a $P2_12_12_1$ space group in agreement with the observed reflection conditions $(h, 0, 0)$ with $h = 2n$, $(0, k, 0)$ with $k = 2n$ and $(0, 0, l)$ with $l = 2n$. It corresponds to 8 molecules in the unit cell and 2 molecules in the asymmetric units. From the refinements, it appeared that one molecule in the asymmetric units was well defined but the other one showed a strong static disorder on the phenyl ring orientation. We should also point out that the hypothesis of a $P2_12_12_1$ space group is not satisfying from the point of view of Landau theory of second order phase transitions. The space group of the intermediate phase should be a subgroup of the β-phase $Pca2_1$ space group (Sect. 5.3), which is not the case for the $P2_12_12_1$ space group. Therefore we made the hypothesis of a $P2_1$ space group for the intermediate phase, which is in agreement with the observed reflection conditions and a group-subgroup relationship between $Pca2_1$ and $P2_1$. The refinement of the structure was however not conclusive: the positions of the atoms of the four molecules in the asymmetric units were not determined. $P2_1$ space group should correspond to a monoclinic unit cell but no significant deviation from a value of 90° for the β angle was observed.

To conclude, we may say that the nondetermination of the crystallographic structure of the intermediate phase is probably due to the fact that the room temperature (T = 295 K) at which the data acquisition was made is too close to the second order phase transition at T_2 = 307 K. The temperature interval between T_1 = 291 K and T_2 = 307 K is too narrow to perform such a study in a satisfactory manner. The fact that there is no group-subgroup relationship between the α- and β-phase or between the α- and intermediate I-phase (see Sect. 4) will be considered in the conclusion (Sect. 8).

5.3 β-phase

Complete structure determination of the ZWT single crystal was performed at two temperatures T = 333 K and T = 375 K (see Tab. 1). They correspond to the orthorhombic β-phase with the $Pca2_1$ space group, 8 molecules in the unit cell (Z = 8) and 2 molecules in the asymmetric units. Contrary to Sarma *et al.* [3], we point out first that the $\alpha \rightarrow \beta$ structural change does not correspond to a cell doubling. In both cases, there are 8 molecules in the unit cell and two molecules in the asymmetric unit. Moreover, both space groups, Pnc2 (α-phase) and $Pca2_1$ (β-phase) correspond to the same point group mm2. The differences between both structures are then expected to be more subtle. In Figure 10, a projection of two adjacent layers of ZWT molecules along the b axis is shown at T = 375 K. By comparison to Figure 9 one may see that the main differences correspond to different arrangements of the phenyl ring orientations (note that the (a, b) plane of the α-phase corresponds to the (a, c) plane of the β-phase). At first, in one stack along the b axis (in Fig. 10), there are two phenyl rings orientations but these two orientations are different from the ones in the corresponding stack of the α-phase (Fig. 9). Second, if one considers for example the upper layer, the main feature is that contrary to the α-phase two different phenyl ring orientations are observed for d+ molecules; an identical feature is observed for the d− molecules in the same layer. If the mean projections of the phenyl rings of the d+ and d− molecules on the (a, c) plane are represented by lines, it appears in Figure 10 that the phenyl rings have the same

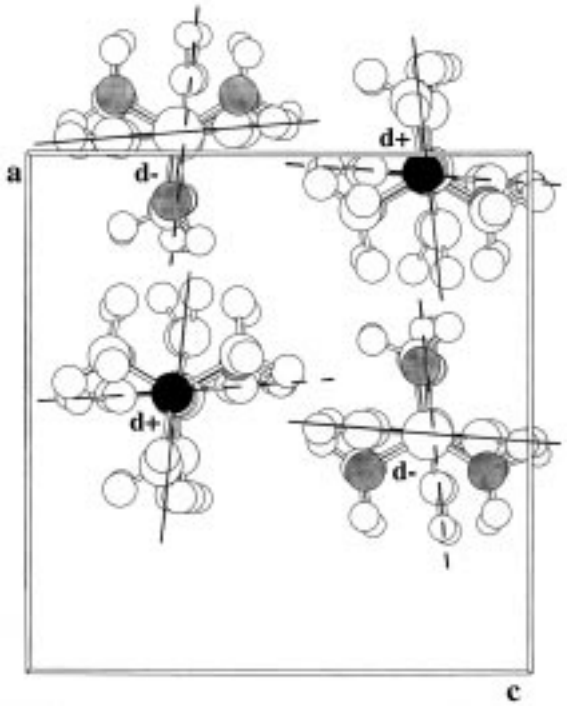

Fig. 10. Projection of two adjacent layers of molecules (contained in the same orthorhombic cell) along the b direction in the β-phase of a ZWT single crystal. The molecules are called d+ (electric dipole up) and d− (electric dipole down). The lines represent the orientations of the phenyl rings perpendicular to the (ac) plane. These orientations are different from those observed in the α-phase (Fig. 9); the dashed lines give the orientations in the lower layer, the full lines in the upper layer.

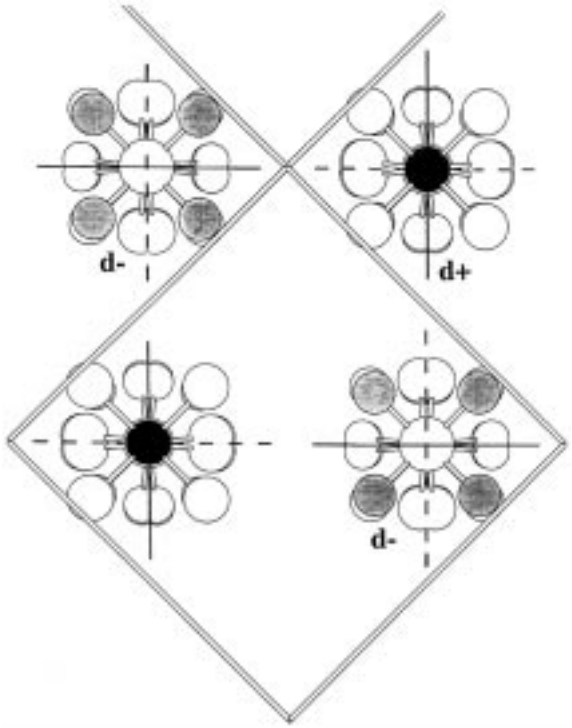

Fig. 11. Projection of two adjacent layers of molecules (in the same tetragonal cell) along the c direction in the γ-phase of a ZWT single crystal. The cell is tilted by 45° to make a better comparison between this arrangement and the ones in the α and β-phase structures (Figs. 9 and 10); the dashed lines give the orientations of the phenyl rings in the lower layer, the full lines in the upper layer.

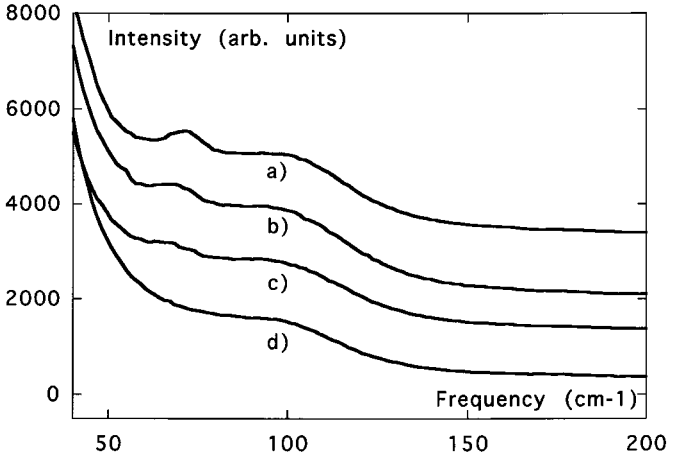

Fig. 12. Low-frequency Raman spectra of a ZWT single crystal (grown from aqueous solution) in the [0–200 cm^{-1}] frequency range at $T = 333$ K (a), $T = 373.5$ K (b), $T = 385.5$ K (c) and $T = 386$ K (d). A mode, located around 70 cm^{-1} on spectra (a), (b) and (c) has disappeared on spectrum (d).

mean orientation in a d+ molecule of the upper layer and in a d− molecule of the lower layer in two consecutive stacks in the b direction; but this same mean orientation is different depending on whether the two consecutive stacks are located on the left or on the right side of the figure. The conclusion is similar for the lower d+ and the upper d− molecules in two consecutive stacks in the b direction.

5.4 γ-phase

Structure determination of the ZWT single crystal was performed at $T = 400$ K: it corresponds to the tetragonal γ-phase (see Tab. 1). The observed reflection conditions were $hk0$ with $h + k = 2n$ and $0kl$ with $l = 2n$ indicating a structure corresponding to the $P4_2/ncm$ space group with 4 molecules in the unit cell ($Z = 4$). Positional parameters for hydrogen atoms were not refined and isotropic thermal parameters were taken for carbon, nitrogen and sulfur atoms. It should be noted that reflection conditions are close to $hk0$ with $h + k = 2n$ and $00l$ with $l = 2n$. A possible $P4_2/n$ space group is obtained by taking into account some weak $0kl$ reflections with $l = 2n$ for $k \neq 0$. Anyway the previous hypothesis of Sarma *et al.* [3] (structure corresponding to the space group P4/nmm with 2 molecules in the unit cell) is not correct. Figure 11 shows a projection of two adjacent layers of molecules along the c direction. The cell in the (a, b) plane was tilted by 45° to make a better comparison to α and β-phase structures (Figs. 9 and 10). It also indicates that the cell doubles in the (a, b) plane at the $\beta \rightarrow \gamma$ phase transition. For being compatible with $P4_2/ncm$ symmetry, an 1/2 occupation factor was assigned to the carbon atoms on the phenyl ring in $(1/4, 1/4)$ positions and 3/4 occupation factor to the carbon atoms and oxygen atoms in the $N(CH_3)^+$ and SO_3^- groups respectively. It is the simplest way to account for the dynamical disorder in the γ-phase (see Sect. 6). It is analogous to the case of H_3NBH_3 where tetragonal observed symmetry is apparently not compatible with the threefold axes of the NH_3 and BH_3 groups [13]. In that case these groups were supposed to behave as axial rotators in order to restore the four fold symmetry.

The data collection already led us to neglect positions of the hydrogen atoms and the anisotropic thermal motions. Nevertheless as stated by Sarma *et al.* [3] the orientational disorder of the $(NCH_3)^+$ and SO_3^- groups enable the reorientation of the phenyl rings (Fig. 11). In one stack, two different mean orientations are observed. These orientations are related by an angle equal to 90°. If the molecules are considered in a single layer, it appears that all d+ molecules correspond to only one phenyl ring orientation and all d− molecules correspond to another one; but the angle between these two orientations is equal to 90°.

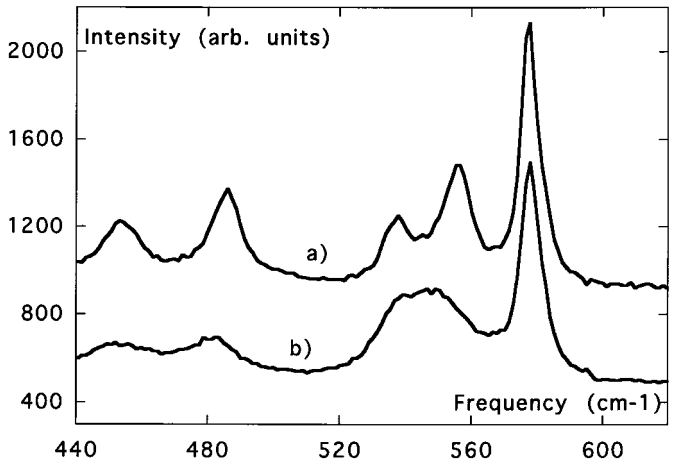

Fig. 13. Raman spectra of a ZWT single crystal (grown from aqueous solution) in the [440–620 cm^{-1}] frequency range at $T = 385.5$ K (a) and $T = 386.5$ K (b). The modes located at 454 cm^{-1}, 486 cm^{-1}, 537 cm^{-1} and 556 cm^{-1} in the β-phase (a) are broadened in the γ-phase (b).

6 Raman scattering study of orthorhombic-tetragonal transition

6.1 Low frequency range [0–150 cm^{-1}]

Figure 12 shows the Raman spectra of a ZWT single crystal (grown from aqueous solution) at respectively $T =$ 333 K, $T = 373.5$ K, $T = 385.5$ K and $T = 386$ K in the [0–200 cm^{-1}] frequency range. The only clear signature of the $\beta \rightarrow \gamma$ phase transition at T_3 temperature is the disappearing of the lattice mode located at about 70 cm^{-1}. A detailed study of its behaviour was not possible because the underlying lattice modes are very broad and the Rayleigh scattering is very significant. Indeed the phase transition temperature $T_3 = 386$ K is a high temperature for a molecular crystal.

6.2 Intermediate frequency range [150–800 cm^{-1}]

Figure 13 shows the Raman spectra at respectively $T =$ 385.5 K and $T = 386.5$ K of a ZWT single crystal grown from aqueous solution in the [440–620 cm^{-1}] frequency range. In this figure modes at 454, 486, 537 and 556 cm^{-1} in the β-phase (Fig. 13a) are broadened and shifted in the γ-phase (Fig. 13b) as indicated in Figure 14b for the mode at 486 cm^{-1}, whereas the frequency of the mode at 578 cm^{-1} is not changed. Indeed, in this frequency range, a mixing between the lattice modes and the torsional modes of the molecules is expected. The modes at 235, 246, 356, 396 cm^{-1} are also affected by the disorder but they are not represented. The frequencies of the modes at 175, 631, 660 and 760 cm^{-1} are not changed.

In Figure 14a, the variation of the width of the 486 cm^{-1} mode (Fig. 13a) is represented as a function of temperature in the [320 K–420 K] temperature range. At the $\beta \rightarrow \gamma$ phase transition, the width undergoes a steep increase from a value of 12 cm^{-1} to a value of 18 cm^{-1}. This increase is characteristic of an order-disorder mechanism [14,15]. Figure 14b shows the variation of the frequency of this mode as a function of temperature. A 3 cm^{-1} discontinuous decrease of the frequency is observed at T_3 from a value of 485.5 cm^{-1} to the value of 482.5 cm^{-1}.

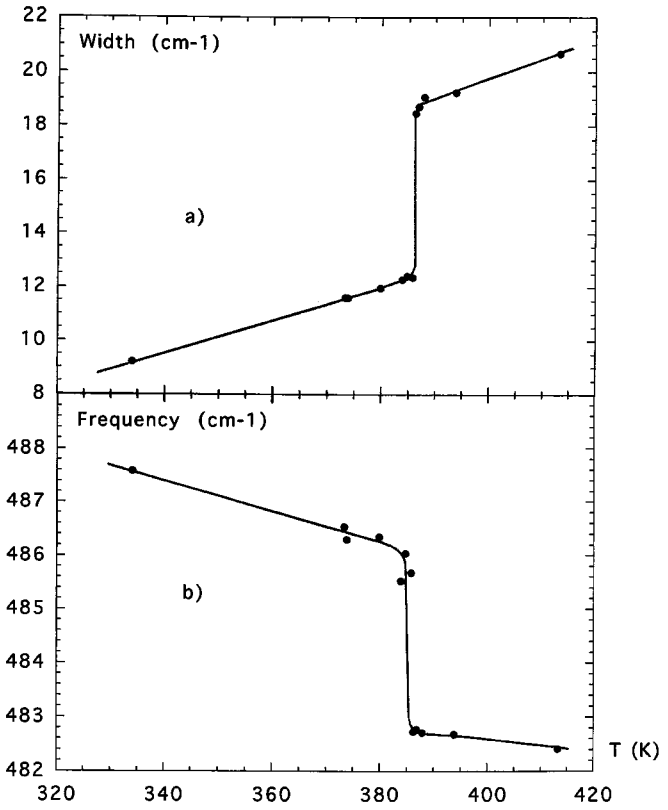

Fig. 14. (a) Evolution of the width of the 486 cm^{-1} mode (shown in Fig. 13a) as a function of temperature in the [320–420 K] temperature range. A steep increase of the width from 12 cm^{-1} to 18 cm^{-1} is observed at T_3. It is characteristic of an order-disorder mechanism. (b) Evolution of the frequency of the 486 cm^{-1} mode (shown in Fig. 13a) as a function of temperature in the [320–420 K] temperature range. A 3 cm^{-1} decrease of the frequency is observed at T_3. The lines are a guide to the eye.

6.3 High frequency range [800–1 250 cm^{-1}]

Figure 15 shows the Raman spectra of a ZWT single crystal grown from aqueous solution at $T = 385.5$ K and $T = 386.5$ K in the [800–1 250 cm^{-1}] frequency range. The modes located at 851, 1 011, 1 044, 1 109, 1 137, 1 209 cm^{-1} are not affected by the $\beta \rightarrow \gamma$ transition. A mode observed as a shoulder at around 1 197 cm^{-1} of the 1 209 cm^{-1} mode in the β-phase (Fig. 15a) disappears in the γ-phase (Fig. 15b). The modes at 945 and 960 cm^{-1} are broaden in the high temperature γ-phase. A spectroscopic comparative study of quaternary ammonium compounds

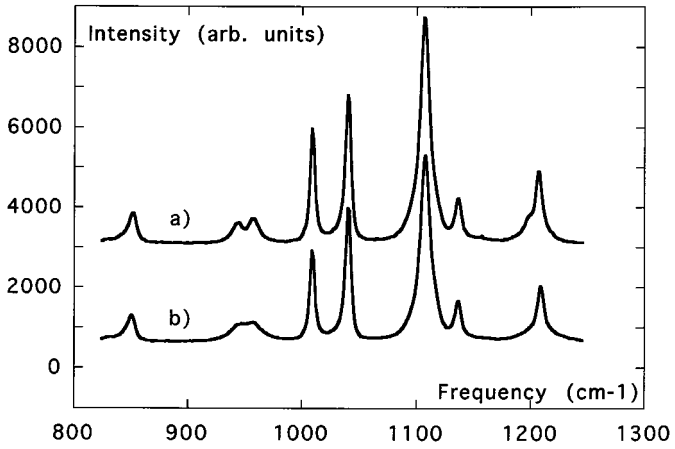

Fig. 15. Raman spectra of a ZWT single crystal (grown from aqueous solution) in the [800–1 250 cm^{-1}] frequency range at $T = 385.5$ K (a) and $T = 386.5$ K (b). The modes located at 945 cm^{-1} and 960 cm^{-1} in the β-phase (a) are broadened in the γ-phase (b).

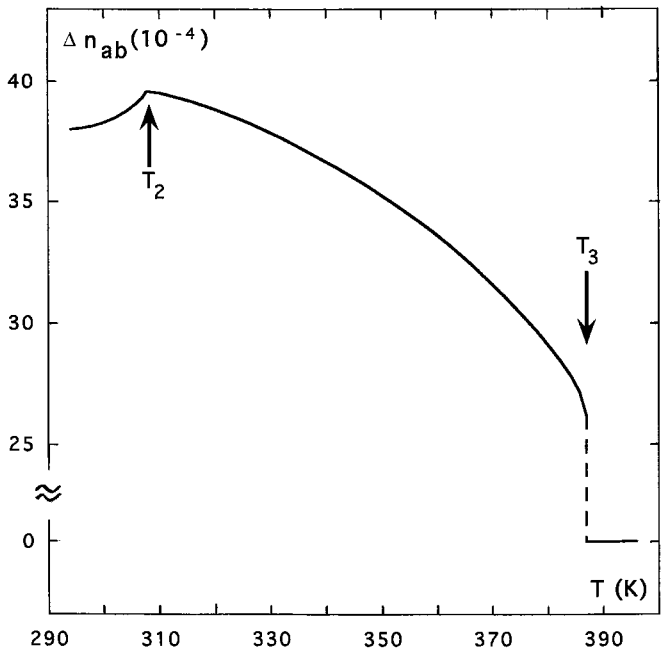

Fig. 16. Evolution of the birefringence Δn_{ab} of a ZWT single crystal as a function of temperature ($\lambda = 0.55$ μm) at heating run with +0.5 K min^{-1} in the [300–400 K] temperature range. The second order phase transition at $T_2 = 307.5$ K and the first order phase transition (with large birefringence discontinuity step: broken line) at $T_3 = 386.5$ K are clearly visible.

R–$N^+(CH_3)_3$ can be found in the literature [16]. The common feature of these compounds is that they have three bands in the [900–980 cm^{-1}] frequency range and at least one band in the [400–480 cm^{-1}]. The authors point out that these frequencies are not easily affected by differences in chemical structure of the substituent group R. The three bands in the [900–980 cm^{-1}] frequency range involve stretching of the C–N^+ bond whereas the band in the [400–480 cm^{-1}] frequency range involves bending of the C–N^+ bonds. For the phenyltrimethyl ammonium ion, which has a chemical structure very near that of ZWT, two very strong bands are observed at 940 and 945 cm^{-1} and a weaker one at 912 cm^{-1}, and also one band at 475 cm^{-1}. In the ZWT molecules, we may conclude, by comparison, that the two modes at 944 cm^{-1} and 959 cm^{-1} involve stretching of the C–N^+ bond, and that the two modes at 454 cm^{-1} and 486 cm^{-1} involve bending of the C–N^+ bonds. It seems to indicate that C–N^+ stretching and bending modes are coupled to the rotation of the $-C(NH_3)_3^+$ group; the $\beta \rightarrow \gamma$ transition would then correspond to the $-C(NH_3)_3^+$ rotational disorder (see Sect. 4).

The Raman spectra of a ZWT sample obtained directly from the MSE → ZWT solid-state reaction and retaining good crystallinity show the same features as the spectra of ZWT samples grown from aqueous solution.

7 Birefringence study

ZWT single crystals in the form of the (*ab*) rectangular plates with parallel extinction (thickness range 25–600 μm) were used in optical birefringence studies.

At 293 K, the birefringence of ZWT crystals within the (*ab*) plane was carefully determined by means of a tilting (Ehringhaus) compensator, and for thicker plates by quantitative analysis of an acute bisectrix-centered interference (conoscopic) figure [12, 17]. The average value thus obtained amounts to only $\Delta n_{ab} = 0.003\,8(3)$ ($\lambda = 0.55$ μm). It is to be noted that this rather small anisotropy in the (*ab*) plane reflects well the molecular arrangement in the crystal (the molecules form a set of polar chains running along the *c*-axis; [3] and Sect. 4). We have also refined our previously reported value of the optic axial angle $2V$ [5] by using a special well tested conoscopic set-up with circularly polarized light to improve the precision. Its value ($T = 291$ K–298 K, $\lambda = 0,55$ μm) amounts to $(+)\ 2V = 26.6 \pm 0.5°$. Both these values (*i.e.* Δn_{ab} and $2V$) are useful and unambiguous characteristics of the RT crystalline structure of ZWT; both were used successfully during crystal optical monitoring of the monocrystalline ZWT regions at a final stage of the solid state MSE → ZWT reaction [5, 18].

Temperature evolution of Δn_{ab} in the [294 K–390 K] range was measured with birefringence resolution of approximately 10^{-5} by means of a tilting (Ehringhaus) compensator with visual inspection (Fig. 16). Heating/cooling runs with a small rate ±0.5 K/min were performed. It is important to note that special attention was given to study only monodomain areas of the samples. The Δn_{ab} *versus* temperature curve obtained (Fig. 16) gives clear evidence of two phase transitions of different character: at $T_2 = 307.5$ K, a second order phase transition (distinct slope change, birefringence reaches its maximum without discontinuity), in agreement with DSC measurements (Sect. 3.1 and Fig. 2); at $T_3 = 386.5 \pm 0.5$ K, a first order phase transition (large discontinuous birefringence

step of *ca.* 26×10^{-4}, thermal hysteresis of *ca.* 0.4 K). The T_3 phase transition characteristics agree well with DSC and Raman scattering studies (Sects. 3.5 and 6) and with literature data [3]. In accordance with calorimetric results (Sect. 3.2) distinguishable optical signs of a reversible phase transition at T_3 are also directly observed in polarized light on ZWT samples after complete thermal conversion of starting MSE monocrystalline plates.

Above T_3, due to tetragonal symmetry of the γ-phase ([3] and Sect. 4), the crystal is optically uniaxial with zero birefringence value within the studied plane (ab). The same feature is observed for ZWT samples obtained directly from the MSE → ZWT reaction and retaining good crystallinity. A large discontinuous step of the $2V$ angle (of estimated value approximately 22 degrees) at T_3 transition was also observed (in agreement with birefringence results).

Further studies in the temperature region below 294 K are planned with the aim to get some optical signature of the T_1 transition. Preliminary results indicate that refraction indices ellipsoid coincides with the crystal axes at the T_2 transition. In the I-phase, extinction directions remain the same within resolution of the experimental set-up (amounting to 0.1 degree) during wavelength changes (visible region) and also during temperature changes. Then it seems to indicate that the I-phase is orthorhombic but the greatest care must be taken in drawing conclusions in a narrow temperature range (T_1, T_2) near a second order transition.

8 Discussion and conclusion

By associating four different experimental techniques (calorimetry, X-ray and Raman scattering, optical birefringence) we have been able to obtain a complete view of the phase transitions in ZWT crystals. The crystal quality (Sect. 2.1) has been improved in comparison to previous studies [3]. It has been shown indeed that diffuse streaks along c^* observed by the authors of reference [3] and attributed to stacking faults are replaced on the X-ray photographs (Sect. 4.3) and in structure determination (Sect. 5) by Bragg peaks. This is consistent with the fact that the calorimetric signatures are well defined in our case for all the transitions. We were then able to confirm some of the tentative conclusions of the previous authors but also to state that some others were wrong. It is, then, possible now to study the disorder in ZWT samples obtained through the thermally induced MSE → ZWT solid state reaction. In addition a new phase was discovered.

From our calorimetric (Figs. 1 and 2) and birefringence (Fig. 16) studies, we may conclude that the α-phase and the β-phase are well separated. The crystallographic structure determinations (Sect. 5) indicate however that the differences are subtle. There is no group-subgroup relationship between the two phases' space groups: Landau theory may not be used. The orientations of the phenyl rings are different in the α-phase and the β-phase but the orientations of the $-N(CH_3)^+$ and SO_3^- groups are the same.

The phenyl rings have two orientations within one stack along the c axis both in the α-phase and the β-phase but relations between two adjacent layers are different. The intermediate new phase between $T_1 = 291$ K and $T_2 = 307$ K corresponds to the reflection conditions of the $P2_12_12_1$ space group. In order to yield a group-subgroup relationship with the $Pca2_1$ space group of the β-phase, the $P2_1$ space group was also considered. Refinements of the X-ray diffraction data were not conclusive. A possible explanation of this failure is that the intermediate phase exists in a too narrow temperature interval. It may explain why, in ZWT crystals of bad quality either grown in methanol-water solutions [3] or obtained by the MSE → ZWT reaction, defects smooth out the intermediate phase. The β-phase is described at room temperature by Sarma *et al.* [3] by averaging over the four orientations of the phenyl ring in the α-phase. Stacking faults were proposed by these authors, as the origin of phenyl ring flip in one layer into one of the four symmetry-related arrangements of the α-phase. This disorder along the c axis is not present in our refinement of the β-phase (Sect. 5.3) and it corresponds to a c parameter value divided by a factor of 2. In ZWT crystals containing a large quantity of defects (Fig. 2b), only a broad endotherm is observed by DSC.

The transition at T_3 between the β-phase and γ-phase now appears as a transition of dynamical nature between an orthorhombic phase and a tetragonal phase. The orientational disorder of the $N(CH_3)_3^+$ and SO_3^- is checked both by X-ray diffraction and Raman scattering. As a consequence phenyl rings are able to adopt orientations which are perpendicular. In α-phase and β-phase the static orientations of the $N(CH_3)_3^+$ and SO_3^- group certainly prevent the phenyl rings from taking the preferred orientations which make an angle equal to 90°. Starting from P4/nmm ($Z = 2$) space group proposed by the authors of reference [3] for the γ-phase, a group-subgroup relationship is found with the $P4_2/ncm$ ($Z = 4$) space group proposed by us for the γ-phase. When comparing both space-groups, one finds that P4/nmm is deduced from $P4_2/ncm$ by averaging two different orientations of the phenyl rings along the c axis. Therefore the c axis parameter for $P4_2/ncm$ is twice the one for P4/nmm. A group-subgroup relationship also exists between the $P4_2/ncm$ ($Z = 4$) space group and the $Pca2_1$ ($Z = 8$) space group (β-phase). One may suppose that such a relation exists between the $Pca2_1$ space group (β-phase) and an hypothetic $P2_1$ space group for the intermediate phase ($Z = 8$). However, a group-subgroup relationship is not possible for the Pnc2 ($Z = 8$) space group of the α-phase, neither with the $Pca2_1$ space group nor with the $P2_1$ or $P2_12_12_1$ space group. Therefore a first order reconstructive phase transition leads from the intermediate phase to the low-temperature α-phase as shown by calorimetry.

However, it is interesting to point out that the Pnc2 space group ($Z = 8$) is a subgroup of P4/nmm, as $P4_2/ncm$, $Pca2_1$ and $P2_1$. Following the definitions of references [19,20], we may consider that the P4/nmm is the common latent parent structure which corresponds

to a statistically disordered solid prototype. In references [19,20] the martensitic fcc-hcp reconstructive phase transition is analyzed as a transition between two low-symmetry ordered phases induced by two different irreducible representations of a common disordered latent parent phase of hexagonal symmetry. In the case of the reconstructive first order phase transition at T_1 in the ZWT crystal, we shall point out that the enthalpy is weak ($\Delta H = 0.73$ J/g), probably because the re-ordering only affects the orientations of the phenyl rings and does not affect greatly the mean positions of the molecules.

Some conclusions about the MSE → ZWT chemical reaction can be deduced from this study. After this reaction is complete, three types of static disorder occur. The first one is a static disorder in the $-N(CH_3)_3^+$ and SO_3^- orientations. In that case, after annealing above 423 K in the γ-phase (Fig. 4a) where dynamical reorientations are observed (Sect. 6), some ordering is restored (Fig. 4b). The second type of disorder concerns the phenyl ring orientations. We know from calorimetric measurements (Sect. 3) that the coupling between the dynamical disorder of $-N^+(CH_3)$ and SO_3^- groups at the β-γ transition and the phenyl ring reorientation may yield a more ordered crystal. Third, it appears from this study that the walls (which mark the boundaries between the small permanent domains (5–10 μm) due to the plastic deformations which take place during the reaction in MSE-ZWT mixed crystals [5,6]) will prevent either good samples (Fig. 3) or bad samples (Fig. 4) of ZWT obtained after complete transformation of MSE monocrystals to show clear thermodynamic signatures at T_1, T_2 and T_3 as observed in ZWT single crystals grown from aqueous solution (Fig. 1). In the case of the crystals obtained by Sarma *et al.* [3], inclusion of methanol or structural defects arising from the chosen crystallization conditions probably induce both the observed twinning and the disordered β and γ phases. It should be noted that the enthalpy value $\Delta H = 10.2$ J/g reported by these authors is far below the one measured in our good quality ZWT monocrystals grown from aqueous solution ($\Delta H = 19.2$ J/g) and also below the one measured in the crystalline ZWT samples which were obtained at the end of the MSE → ZWT reaction ($\Delta H = 13.2$ J/g). The value $\Delta H = 10.2$ J/g is only of the same order of the one ($\Delta H = 10.0$ J/g) measured in ZWT powders obtained from the MSE → ZWT reaction. The coincidence between the $\Delta S = 5.9\ \mathrm{J\,mol^{-1}\,K^{-1}}$ in reference [3] and $R \ln 2$ is probably accidental, because in our case the ΔS value is far above $R \ln 2$.

To conclude, we may say from this study that we get a clearer view of the phase transitions in ZWT samples and some information about the MSE → ZWT chemical reaction. The good quality of our samples will help us to clarify the structure of the ferroelastic domains below the temperature T_3. Experimental studies are in progress to try to solve this question.

Acknowledgement is made to P. Rabiller for his help at several stages of the X-ray precession study.

References

1. C.N. Sukenik, J.A.P. Bonapace, N.S. Mandel, P.Y. Lau, G. Wood, R.G. Bergman, J. Am. Chem. Soc. **99**, 851 (1977).
2. J.A.R.P. Sarma, J.D. Dunitz, Acta Cryst. B **46**, 780 (1990).
3. J.A.R.P. Sarma, J.D. Dunitz, Acta Cryst. B **46**, 784 (1990).
4. J. Even, M. Bertault, A. Girard, Y. Délugeard, Y. Marqueton, Chem. Phys. Lett. **267**, 585 (1997).
5. J. Even, M. Bertault, J. Gallier, A. Girard, Y. Délugeard, W.J. Kusto, Chem. Phys. Lett. **279**, 319 (1997).
6. J. Even, M. Bertault, J. Gallier, A. Girard, Y. Délugeard, C. Ecolivet, S. Beaufils, L. Toupet, W.J. Kusto, Mol. Cryst. Liq. Cryst. **313**, 135 (1998).
7. M. Bertault, J. Even, Mol. Cryst. Liq. Cryst. **313**, 315 (1998).
8. M. Oda, N. Sato, Chem. Phys. Lett. **275**, 40 (1997).
9. J. Boerio-Goates, J.I. Artman, D. Gold, J. Phys. Chem. Solids **48**, 1185 (1987).
10. Enraf Nonius CAD-4 Operations Manual, Enraf-Nonius, Delft, The Netherlands (1977).
11. G.M. Sheldrick, SHELXL93. Program for the Refinement of Crystal Structures, University of Göttingen, Germany (1993).
12. T.G. Rochow, P.A. Tucker, *Introduction to Microscopy by Means of Light, Electrons, X-ray or Acoustics* (Plenum Press, New-York, London, 1994).
13. E.L. Lippert, W.N. Lipscomb, J. Am. Chem. Soc. **78**, 503 (1955).
14. A. Girard, Y. Délugeard, H. Cailleau, J. Phys. France **48**, 1751 (1987).
15. J. Even, M. Bertault, B. Toudic, H. Cailleau, J.L. Fave, R. Currat, F. Moussa, Phys. Rev. B **49**, 1602 (1994).
16. A.S. Hume, W.C. Holland, F. Fry, Spectrochim. Acta A **24**, 786 (1968).
17. W.J. Kusto, J.P. Rivera, H. Schmid, Ferroelectr. **125**, 191 (1992).
18. W.J. Kusto, M. Bertault, J. Even, J. Phys. Chem. (in press).
19. V.P. Dimitriev, S.B. Rochal, Y.M. Gufan, P. Tolédano, Phys. Rev. Lett. **62**, 2495 (1989).
20. Yu.A. Izyumov, V.N. Syromyatnikov, *Phase Transitions and Crystal Symmetry* (Kluwer Academic Publishers, Dordrecht-Boston-London, 1990).